

Fine-tuning and vacuum stability in Wilsonian effective action

Tomasz Krajewski* Zygmunt Lalak†

Institute of Theoretical Physics, Faculty of Physics, University of Warsaw
ul. Pasteura 5, Warsaw, Poland

Abstract

We have computed Wilsonian effective action in a simple model containing scalar field with quartic self-coupling which interacts via Yukawa coupling with a Dirac fermion. The model is invariant under a chiral parity operation, which can be spontaneously broken by a vev of the scalar field. We have computed explicitly Wilsonian running of relevant parameters which makes it possible to discuss in a consistent manner the issue of fine-tuning and stability of the scalar potential. This has been compared with the typical picture based on Gell-Mann–Low running. Since Wilsonian running includes automatically integration out of heavy degrees of freedom, the running differs markedly from the Gell-Mann–Low version. However, similar behavior can be observed: scalar mass squared parameter and the quartic coupling can change sign from a positive to a negative one due to running which causes spontaneous symmetry breaking or an instability in the renormalizable part of the potential for a given range of scales. However, care must be taken when drawing conclusions, because of the truncation of higher dimension operators. Taking scalar field’s amplitude near the cut-off Λ may cancel suppression due to the scale and only suppression due to small couplings partially justifies truncation in this region. Also, when taking the cut-off higher, to include larger amplitudes of the fields, higher-order irrelevant operators, whose coefficients grow with scale, may affect the conclusion about stability. The Gell-Mann–Low running allows one to resume relatively easily a class of operators corresponding to large logarithms to form the RGE improved effective potential valid over a huge range of scales. In the Wilsonian approach this would correspond to following the running of a large number of irrelevant operators, which is technically problematic. As for the issue of fine-tuning, since in the Wilsonian approach power-law terms are not subtracted, one can clearly observe the quadratic sensitivity of fine-tuning measure to the change of the cut-off scale.

1 Introduction

The recent discovery of the Higgs boson at the Large Hadron Collider [1, 2] promotes the question about protection of the electroweak breaking scale to one of the most puzzling problems of fundamental physics. The observed compatibility of properties of the newly observed particle with predictions coming from Standard Model additionally strengthens tension between standard theoretical reasoning which results in prediction of new physics near the electroweak scale and reality. Neither supersymmetry nor composite Higgs models, perhaps most attractive solutions to hierarchy

*Tomasz.Krajewski@fuw.edu.pl

†Zygmunt.Lalak@fuw.edu.pl

problem, are favored by the observed value of Higgs mass [3, 4, 5]. Moreover, production and decay rates (measured within large errors so far) have not provided unambiguous evidence for new physics.

This situation strengthens the need of revisiting the naturalness principle which have been used as a guide for model building, since its formulation in the late 1970s and early 1980s [6, 7, 8]. Numerous authors [9, 10, 11, 12, 13, 14, 15] propose new definitions of naturalness. Our goal is less ambitious. We shall try to state clearly a treatment of fine-tuning based on Wilsonian effective action and corresponding Wilsonian renormalization group. Idea of Wilsonian effective action is close to the intuitive understanding of cutoff regularization. In standard discussion based on quadratic divergences the artificial meaning of a scale of effective theory is given to the regularization parameter Λ . This effects in the regularization dependence of this kind of analysis. On the contrary, in the Wilsonian method high energy modes are integrated out in a self consistent, regularization independent way and effective theory has a well-defined effective action. Moreover, this treatment is universal and depends very weakly on a preferred UV completion (quantum gravity, string theory, etc.). Main impact on effective action from states with masses greater than the scale of the effective theory can be parameterized by values of couplings of the Wilsonian effective action. Further corrections are highly suppressed as far as heavy masses are separated from the scale of the effective theory.

Given a model where vacuum expectation value of a scalar field can be generated with quantum corrections we can also show how the stability of the effective action looks like from the point of view of Wilsonian running. This has been compared with the typical picture based on Gell-Mann–Low running known from the Standard Model. Since Wilsonian running includes automatically integration out of heavy degrees of freedom, the running differs markedly from the Gell-Mann–Low version. However, similar behavior can be observed: scalar mass squared parameter and the quartic coupling can change sign from a positive to a negative one due to running which causes spontaneous symmetry breaking or an instability in the renormalizable part of the potential for a given range of scales. However, care must be taken when drawing conclusions, because of the truncation of higher dimension operators.

The paper is organized as follows. In Section 2 we specify the model and define truncation. We argue in Subsection 2.1 that this model should present behavior similar to that of SM. In Subsection 2.2 we show in what sense the RGE for chosen truncation can be thought as a analogue of 1-loop running of Gell-Mann–Low type. In Section 3 we present calculated RGE which numerical solution is discussed in Section 4. Section 5 is dedicated to numerical estimation of fine-tuning of parameters of Wilsonian effective action. In Section 6 we discuss the issue of radiative stability of the effective action and in 7 we summarize our results. Appendix A contains brief introduction to Wilsonian RGE and Functional Renormalization Group methods. The derivatives of loop integrals used during calculations are given in Appendix B. In Appendix C matching conditions which gives parameters of Wilsonian effective action in terms of measurable quantities are given.

2 Basic features of the model

2.1 Lagrangian couplings

For the sake of clarity and technical simplicity of our considerations it is convenient to consider a model that is much simpler than the Standard Model, but exhibits certain interesting features

similar to those known from the SM. We pick up a model in which a massless Dirac fermion Ψ couples via Yukawa interaction to a real scalar field Φ with a quartic self-coupling. This theory can be described by a classical Lagrangian density of the form:

$$\mathcal{L} = i\bar{\Psi}\not{\partial}\Psi + \frac{1}{2}\partial_\mu\Phi\partial^\mu\Phi - \frac{1}{2}M^2\Phi^2 - Y\Phi\bar{\Psi}\Psi - \frac{\lambda}{4!}\Phi^4. \quad (2.1)$$

Lagrangian density (2.1) is symmetric under (chiral) \mathbb{Z}_2 acting on Φ as $\Phi \rightarrow -\Phi$ and on Ψ as $\Psi \rightarrow \gamma^5\Psi$. We consider the case of non-zero vacuum expectation value for the field Φ , which breaks this symmetry spontaneously. In broken symmetry phase the Lagrangian density (2.1) will take the form:

$$\mathcal{L} = i\bar{\Psi}\not{\partial}\Psi - m\bar{\Psi}\Psi + \frac{1}{2}\partial_\mu\Phi\partial^\mu\Phi - \frac{1}{2}M^2\Phi^2 - Y\Phi\bar{\Psi}\Psi - \frac{g_3}{3!}\Phi^3 - \frac{\lambda}{4!}\Phi^4. \quad (2.2)$$

The fermion Ψ allows one to model top quark coupling to Higgs boson, which is known to give the main contribution to quadratic divergences in the mass of the SM scalar and to high-scale instability of the quartic coupling. The massless Ψ can obtain a mass from the vev of Φ . We use Dirac fermion instead of a Weyl fermion in order to avoid introducing chiral formalism for the latter. However, all results can be easily extended to such a situation. Gauge interactions have been neglected to avoid additional complications in calculating Wilsonian RGE posed by gauge invariance.

2.2 Perturbative derivation of RGE

We have calculated Wilsonian renormalization group equations in theory described in Section 2.1 at the lowest non-trivial order. The Wilsonian action can include an infinite number of non-renormalizable operators, however they are suppressed at the low cut-off scale. Hence our truncation contains the following operators:

$$\mathcal{L}_\Lambda = i\bar{\Psi}_\Lambda\not{\partial}\Psi_\Lambda + \frac{1}{2}\partial_\mu\Phi_\Lambda\partial^\mu\Phi_\Lambda - \frac{1}{2}M_\Lambda^2\Phi_\Lambda^2 - Y_\Lambda\Phi_\Lambda\bar{\Psi}_\Lambda\Psi_\Lambda - \frac{\lambda_\Lambda}{4!}\Phi_\Lambda^4. \quad (2.3)$$

We define Wilson coefficients M_Λ^2 , Y_Λ and λ_Λ as values of respectively two-, three- and four- point Green's functions at the kinematic point with vanishing external momenta. We use following graphics for cutoff propagator of a scalar field

$$\cdots\cdots\cdots = \frac{\theta_0(p)}{p^2 + M_\Lambda^2} \quad (2.4)$$

and a fermionic field

$$\Rightarrow = \frac{\theta_0(p)}{\not{p} + m_\Lambda}. \quad (2.5)$$

In the diagrams lines $\cdots\cdots\cdots$ and \Rightarrow represent respectively scalar and fermionic low-energy modes.

2.3 Lowest order calculation

The RGE that we obtain can be thought of as an analogue of 1-loop Gell-Mann–Low type RGE. Let us for a moment assume that we add an operator Φ^6 to truncation (2.3). Its lowest-order contribution to β -function for λ comes from diagrams with loop propagator starting and ending in the same vertex. For a theory with bare Lagrangian density of the form (2.1) the operator Φ^6 must be, in standard treatment, generated by loop diagrams. Diagrams given in Fig. 1a and Fig. 1b show the lowest order contribution to Wilsonian coefficient of the Φ^6 operator. These contributions are



Figure 1: Lowest order diagrams which contribute to generating Φ^6 operator in effective Lagrangian density from bare Lagrangian density (2.1).

respectively proportional to λ^3 and Y^6 . Lowest order contribution to β -function for the coupling λ given by the Φ^6 operator comes from loop diagram shown in Fig. 2. Combining diagrams 1 and 2 we

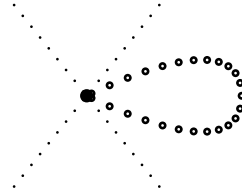


Figure 2: Lowest order contribution to β -function for coupling λ from Φ^6 operator.

obtain 2-loop diagrams given in Fig. 3. To sum up, operator Φ^6 is generated at one loop level and

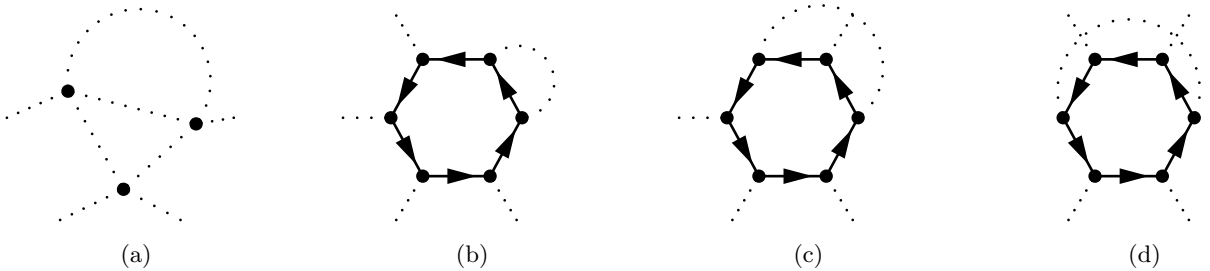


Figure 3: 2-loop contribution to Gell-Mann–Low type running of λ which appear in Wilsonian running as a contribution from Φ^6 and higher dimension operators.

the second loop is needed to obtain contribution to the β -function for λ . The lowest order non-trivial

contributions to Gell-Mann–Low type β -function are of the order λ^2 and Y^4 . The contribution to Wilsonian RGE generated by the operator Φ^6 appears at the 2-loop level in the Gell-Mann–Low type RGE.

On the other hand, we neglected all higher dimension operators with derivatives, for example $\partial_\mu \Phi \partial^\mu \Phi \Phi^2$. It is an easy task to check that the diagram from Fig. 4 gives momentum-dependent¹ contribution to scalar self-energy. More precisely, contribution coming from diagram 4 depends on



Figure 4: Fermion loop diagram that gives momentum-dependent contribution to scalar self-energy.

momentum squared p^2 logarithmically. To recover this dependence from the effective action one needs to consider an infinite number of operators of the form $\Box^n \Phi^2$: $n = 2, \dots$. All these operators are irrelevant near the Gaussian point (the free theory).

3 Flow equations

3.1 Calculating RGE using Mathematica

Our procedure of calculating β functions is as follows:

1. Draw all 1PI and counterterms diagrams with certain number of external fields and write down formal expressions for them.
2. Expand loop integrals in series of external momenta and choose interesting terms (for vertex corrections we set external momenta to zero).
3. Represent loop integrals as standard Passarino–Veltman [16] functions.
4. Express Passarino–Veltman functions in terms of functions I_N with IR cutoff Λ introduced in [17].
5. Differentiate result with respect to Λ . This step gives expressions in terms of derivatives of I_N functions.
6. Substitute derivatives of I_N functions by expressions given in Appendix B.

We have assumed such a procedure for two reasons. Firstly, by calculating effective action before differentiation with respect to cutoff Λ we avoided problems connected with a sharp cutoff derivative (however, one must perform detailed calculation of derivatives with respect to external momenta). Secondly, this algorithm is easy to implement using FeynArts [18] and FeynCalc [19]. FeynArts can easily generate 1-loop 1PI diagrams for the Lagrangian density, which we use as an input for

¹Diagram 4 depends on external momentum of a scalar if we integrate over all modes or just a part of fermionic modes in the loop.

FeynRules [20]. FeynCalc without any modification of source code calculates Passarino–Veltman representation of diagrams generated by FeynArts. Finally we substitute (using Mathematica package modeled after ANT package [21]) Passarino–Veltman integrals by their derivatives with respect to cutoff Λ which we calculated in advance. Calculations performed in Mathematica provide a cross-check for calculations made by hand.

3.2 RGE for the model

As we discuss in the Appendix A.2 it is convenient to express Wilsonian RGE in terms of dimensionless parameters. We use dimensionless parameters $\nu_\Lambda := \frac{v_\Lambda}{\Lambda}$, $\Omega_\Lambda^2 := \frac{M_\Lambda^2}{\Lambda^2}$, $\omega_\Lambda := \frac{m_\Lambda}{\Lambda}$ and $\gamma_3 := \frac{g_3}{\Lambda}$. We define ν_Λ by the requirement that the shift $\Phi \rightarrow \Phi - \nu_\Lambda$ gives effective action without \mathbb{Z}_2 -odd terms.

Derivatives with respect to the scale Λ of the diagrams from Figs. 5, 7, 6, 8, 9 and 10 give flow equations respectively for vacuum expectation value of Φ field, masses of scalar Φ and fermion Ψ , Yukawa coupling, Wilson coefficient g_3 for the operator Φ^3 and the coupling λ . In addition we determine the scaling of fields from diagrams given in Figs. 7 and 6. The RGE read as follows:

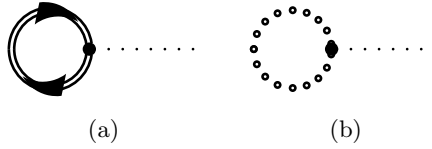


Figure 5: Tadpole diagrams which give contribution to running of ν_Λ parameter.

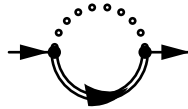


Figure 6: Feynman diagram which give contribution to running of the fermion Ψ mass parameter m_Λ and field renormalization.

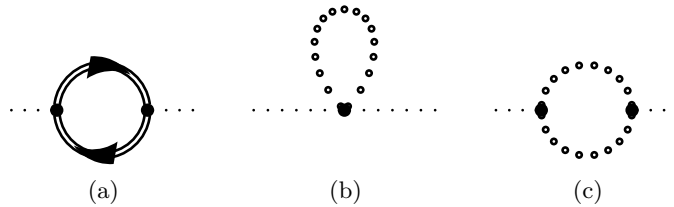


Figure 7: Feynman diagrams which give contribution to running of the scalar Φ mass squared parameter M_Λ^2 and field renormalization.

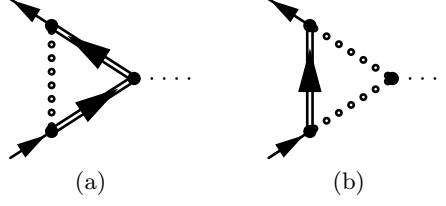


Figure 8: Feynman diagrams which give contribution to running of the Yukawa coupling Y_Λ .

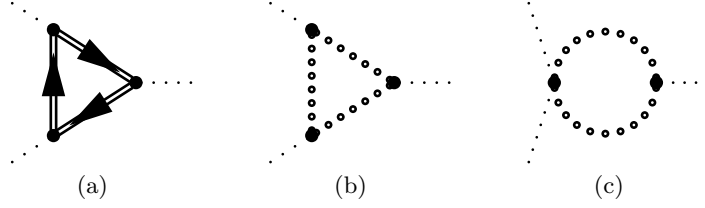


Figure 9: Feynman diagrams which give contribution to running of the parameter $g_{3\Lambda}$ in the ordered phase.

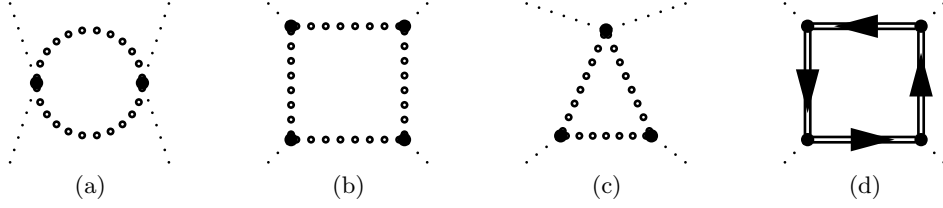


Figure 10: Feynman diagrams which give contribution to running of the Wilson coefficient λ_Λ for the operator Φ^4 .

$$\Lambda \frac{d\nu_\Lambda}{d\Lambda} = -\nu_\Lambda + \frac{1}{\Omega_\Lambda^2} \left[\frac{8Y_\Lambda}{(4\pi)^2} \frac{\omega_\Lambda}{(1+\omega_\Lambda^2)} - \frac{\gamma_{3\Lambda}}{(4\pi)^2} \frac{1}{(1+\Omega_\Lambda^2)} \right] - \frac{\nu_\Lambda}{2} \left[4 \frac{Y_\Lambda^2}{(4\pi)^2} \frac{(3-\omega_\Lambda^2)(1+4\omega_\Lambda^2)}{3(\omega_\Lambda^2+1)^3} \Omega_\Lambda^2 + \frac{\gamma_{3\Lambda}^2}{3(4\pi)^2} \frac{2\Omega_\Lambda^2-1}{(1+\Omega_\Lambda^2)^3} \right]. \quad (3.1)$$

$$\Lambda \frac{d\omega_\Lambda}{d\Lambda} = -\omega_\Lambda - \frac{2Y_\Lambda^2\omega_\Lambda}{(4\pi)^2} \left[\frac{1}{(1+\Omega_\Lambda^2)(1+\omega_\Lambda^2)} - \frac{1}{(1+\Omega_\Lambda^2)(\Omega_\Lambda^2-\omega_\Lambda^2)} + \frac{1}{(\Omega_\Lambda^2-\omega_\Lambda^2)^2} \log \left(\frac{1+\Omega_\Lambda^2}{1+\omega_\Lambda^2} \right) \right] - Y_\Lambda \left[\frac{8Y_\Lambda}{(4\pi)^2} \frac{\omega_\Lambda}{(1+\omega_\Lambda^2)} - \frac{\gamma_{3\Lambda}}{(4\pi)^2} \frac{1}{(1+\Omega_\Lambda^2)} \right] \quad (3.2)$$

$$\begin{aligned} \Lambda \frac{d\Omega_\Lambda^2}{d\Lambda} = & -2\Omega_\Lambda^2 + 4 \frac{Y_\Lambda^2}{(4\pi)^2} \left[\frac{(3 - \omega_\Lambda^2)(1 + 4\omega_\Lambda^2)}{3(\omega_\Lambda^2 + 1)^3} \Omega_\Lambda^2 - \frac{2\omega_\Lambda^2 - 2}{(\omega_\Lambda^2 + 1)^2} \right] \\ & + \frac{\lambda_\Lambda}{(4\pi)^2} \frac{1}{(\Omega_\Lambda^2 + 1)} + \frac{\gamma_{3\Lambda}^2}{(4\pi)^2} \left[\frac{2}{3} \frac{1}{1 + \Omega_\Lambda^2} - \frac{2}{3} \frac{1}{(1 + \Omega_\Lambda^2)^2} + \frac{\Omega_\Lambda^2}{(1 + \Omega_\Lambda^2)^3} \right] \\ & - \gamma_{3\Lambda} \left[\frac{8Y_\Lambda}{(4\pi)^2} \frac{\omega_\Lambda}{(1 + \omega_\Lambda^2)} - \frac{\gamma_{3\Lambda}}{(4\pi)^2} \frac{1}{(1 + \Omega_\Lambda^2)} \right] \end{aligned} \quad (3.3)$$

$$\begin{aligned} \Lambda \frac{dY_\Lambda}{d\Lambda} = & \frac{Y_\Lambda^3}{(4\pi)^2} \left[\frac{\omega_\Lambda^2 - 1}{(\omega_\Lambda^2 + 1)^2 (\Omega_\Lambda^2 + 1)} - \frac{8}{3(\omega_\Lambda^2 + 1)} + \frac{38}{3(\omega_\Lambda^2 + 1)^2} - \frac{6}{3(\omega_\Lambda^2 + 1)^3} \right. \\ & \left. + \frac{2}{(\Omega_\Lambda^2 - \omega_\Lambda^2)^2} \log \left(\frac{\Omega_\Lambda^2 + 1}{\omega_\Lambda^2 + 1} \right) - \frac{2}{(\Omega_\Lambda^2 + 1)(\Omega_\Lambda^2 - \omega_\Lambda^2)} \right] \\ & + \frac{\gamma_{3\Lambda}^2 Y_\Lambda}{(4\pi)^2} \left[\frac{1}{3} \frac{1}{(\Omega_\Lambda^2 + 1)^2} - \frac{1}{2} \frac{1}{(\Omega_\Lambda^2 + 1)^3} \right] - \frac{2\gamma_{3\Lambda} Y_\Lambda^2}{(4\pi)^2} \frac{\omega_\Lambda}{(1 + \Omega_\Lambda^2)(1 + \omega_\Lambda^2)} \end{aligned} \quad (3.4)$$

$$\begin{aligned} \Lambda \frac{d\gamma_{3\Lambda}}{d\Lambda} = & -\gamma_{3\Lambda} + \frac{3\gamma_{3\Lambda}\lambda_\Lambda}{(4\pi)^2} \frac{1}{\Omega_\Lambda^2 + 1} - \frac{7\gamma_{3\Lambda}^3}{2(4\pi)^2} \frac{1}{(\Omega_\Lambda^2 + 1)^3} - \frac{Y_\Lambda^3 \omega_\Lambda}{(4\pi)^2} \frac{16(3 - \omega_\Lambda^2)}{(\omega_\Lambda^2 + 1)^3} \\ & + \frac{\gamma_{3\Lambda} Y_\Lambda^2}{(4\pi)^2} \frac{2(3 - \omega_\Lambda^2)(1 + 4\omega_\Lambda^2)}{(\omega_\Lambda^2 + 1)^3} - \lambda_\Lambda \left[\frac{8Y_\Lambda}{(4\pi)^2} \frac{\omega_\Lambda}{(1 + \omega_\Lambda^2)} - \frac{\gamma_{3\Lambda}}{(4\pi)^2} \frac{1}{(1 + \Omega_\Lambda^2)} \right] \end{aligned} \quad (3.5)$$

$$\begin{aligned} \Lambda \frac{d\lambda_\Lambda}{d\Lambda} = & 3 \frac{\lambda_\Lambda^2}{(4\pi)^2} \frac{1}{(1 + \Omega_\Lambda^2)^2} - \frac{2Y_\Lambda^4}{(4\pi)^2} \left[\frac{1}{(1 + \omega_\Lambda^2)^2} - 8 \frac{\omega_\Lambda^2}{(1 + \omega_\Lambda^2)^4} \right] + \frac{8\lambda_\Lambda Y_\Lambda^2}{3(4\pi)^2} \frac{(3 - \omega_\Lambda^2)(1 + 4\omega_\Lambda^2)}{(1 + \omega_\Lambda^2)^3} \\ & + \frac{6\gamma_{3\Lambda}^4}{(4\pi)^2} \frac{1}{(\Omega_\Lambda^2 + 1)^4} + \frac{2\gamma_{3\Lambda}^2 \lambda_\Lambda}{(4\pi)^2} \left[\frac{2}{3} \frac{1}{(\Omega_\Lambda^2 + 1)^2} - \frac{7}{(\Omega_\Lambda^2 + 1)^3} \right]. \end{aligned} \quad (3.6)$$

4 Numerical solutions of RGE

The RGE (3.2) has been solved numerically. We used matching conditions given in Appendix C to compute initial conditions for the RGE at $\Lambda = 100$ (we use units of GeV through the paper) in terms of physical quantities (see Appendix C for definitions) with renormalization scale $\mu = 100$. The example solution with values: $m_{ph} = 174$, $M_{ph} = 125$, $\lambda_{ph} = 0.2$, $v_{ph} = 264$, $g_{3ph} = 52.8$ and $Y_{ph} = 1$ is presented in the Fig. 11. Double-logarithmic plot 11 shows parameters of the effective Wilsonian action as functions of the scale Λ . Orange line represents Yukawa coupling Y_Λ which runs typically rather slowly. Gray line corresponds to the quartic coupling λ_Λ . This coupling runs faster, because of the contribution from the fermionic loop. Couplings ω_Λ (green line), Ω_Λ^2 (red line) and $\gamma_{3\Lambda}$ (cyan line) for low values of Λ run like relevant couplings due to rescaling, but after reaching scales of the order of the masses, they change their behavior to a slow running near constant value. The behavior of the above couplings for high vales of Λ is caused by the quadratic divergences (or

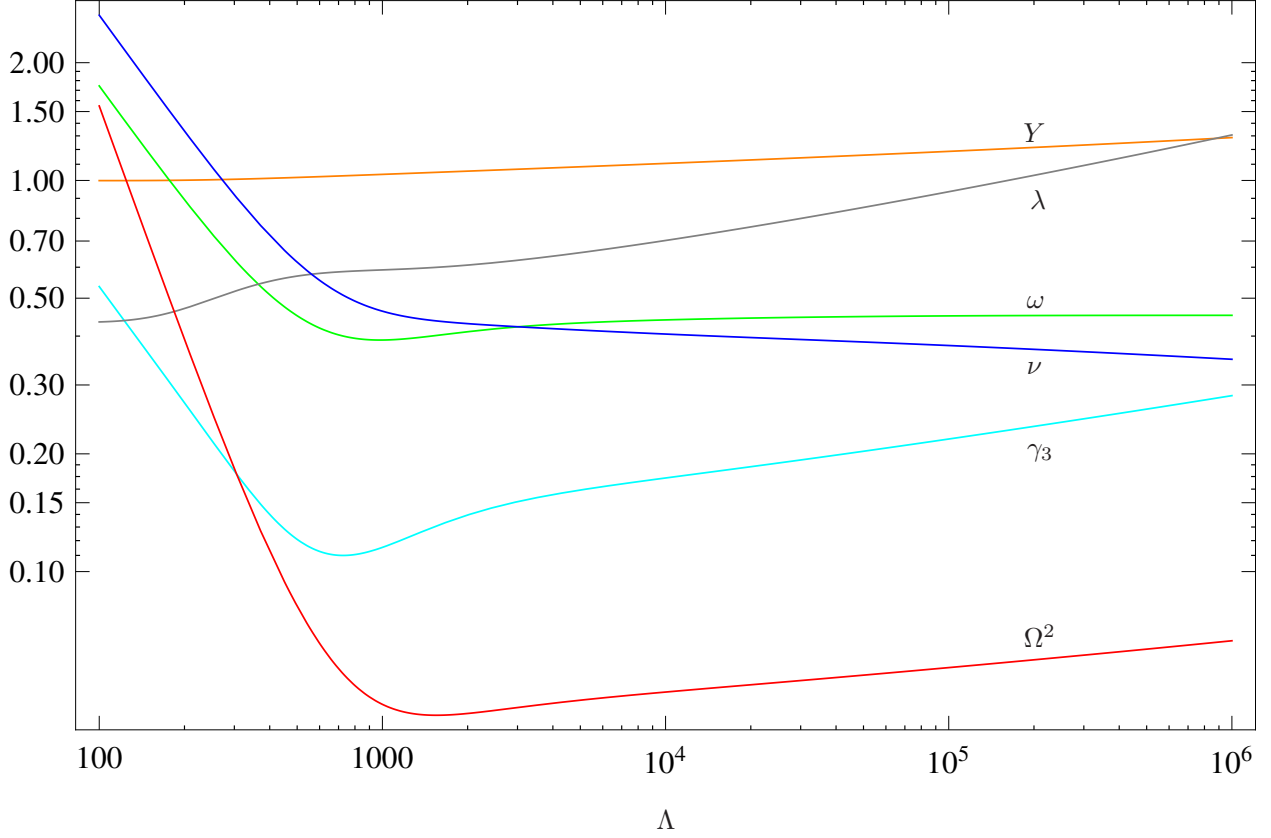


Figure 11: Example of numerical solution of RGE corresponding to: $m_{ph} = 174$, $M_{ph} = 125$, $\lambda_{ph} = 0.2$, $v_{ph} = 264$, $g_{3ph} = 52.8$ and $Y_{ph} = 1$.

more precisely by the same diagrams which generate quadratic divergences). The same behavior is manifested by vacuum expectation value ν_Λ plotted as the blue line.

Solutions with different initial conditions have the same qualitative behavior. In the Fig. 12 we plotted families of solutions with a single parameter varied: the solution with a physical quantity multiplied by $\frac{3}{4}$ and another one with the same parameter multiplied by $\frac{4}{3}$. Reference solution has been plotted as well. Fig. 12a shows solutions with initial conditions $m_{ph} = \frac{3}{4}174$ and $m_{ph} = \frac{4}{3}174$. For solutions presented in Figs. 12b, 12c and 12d we have respectively changed M_{ph} , g_{3ph} and λ_{ph} . In all plots we use the same colors as in Fig. 11 to indicate the same or analogous parameters.

The important observation is that all presented solutions give values very close to each other for Λ of the order of 10^6 . Small change of parameters in effective action at high scale generates physical parameters orders of magnitude different, since the solutions corresponding to different low-scale parameters run very closely to each other when the scale grows. This is the sign that a fine-tuning of parameters in effective action at high scales is required in order to get the prescribed values of physical observables.

The example of numerical solution for the Gell-Mann–Low type RGE for the same theory is

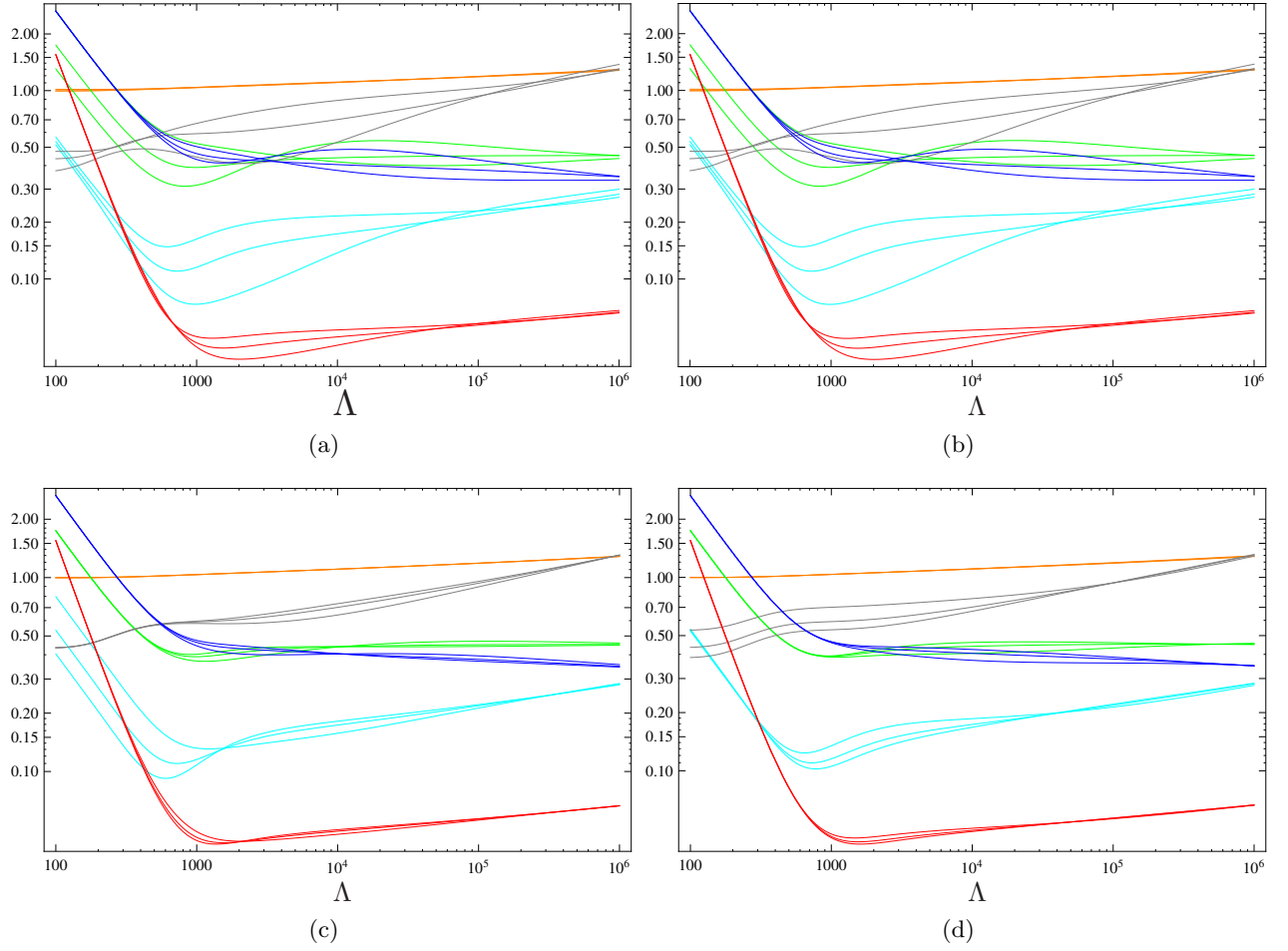


Figure 12: Solutions for changed initial conditions respectively: 12a m_{ph} , 12b M_{ph} , 12c g_{3ph} and 12d λ_{ph} multiplied or divided by the factor $\frac{3}{4}$.

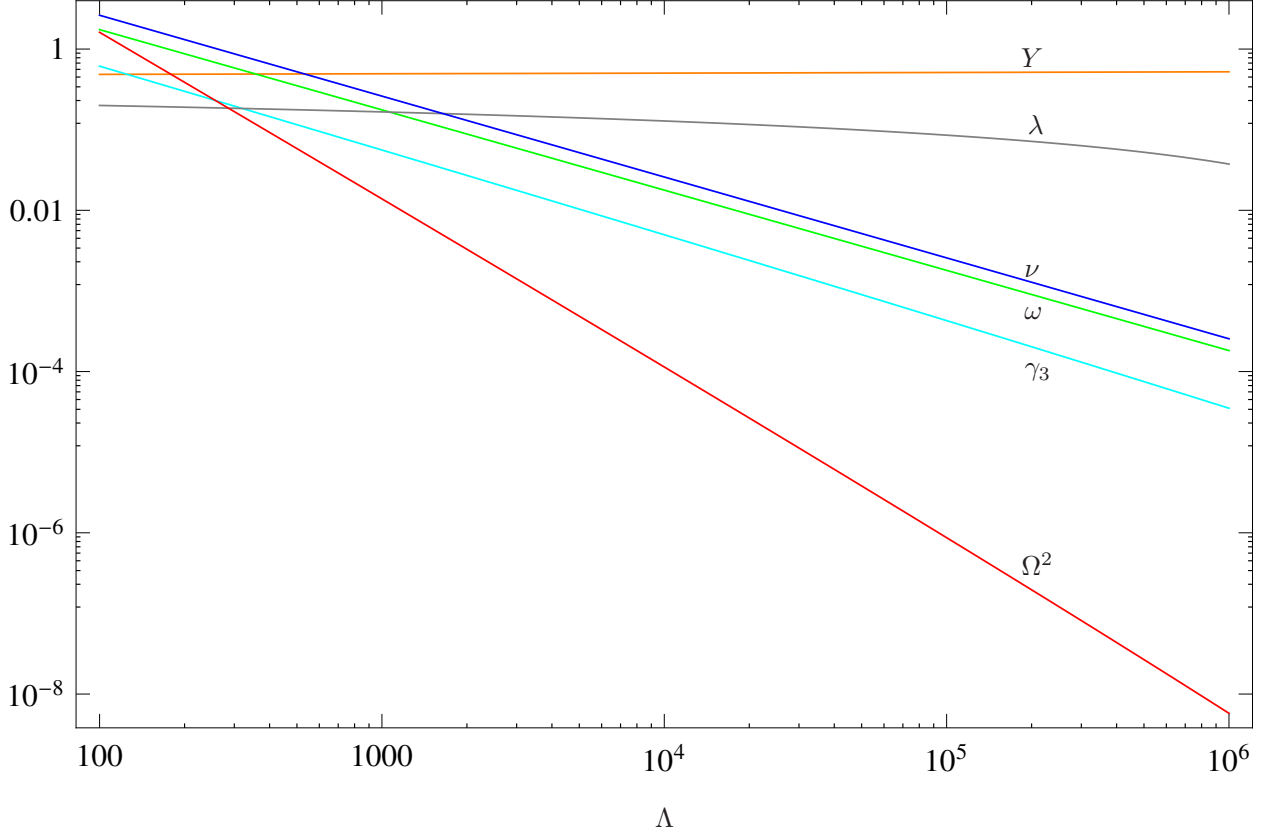


Figure 13: Numerical solution of Gell-Mann–Low type RGE for discussed model corresponding to: $m_{ph} = 174$, $M_{ph} = 125$, $\lambda_{ph} = 0.2$, $v_{ph} = 264$, $g_{3ph} = 52.8$ and $Y_{ph} = 0.5$.

given in Fig. 13. Comparing 13 with 11 one finds that flow of parameters of Wilsonian effective action is much more complicated than the running in the Gell-Mann–Low method. One should note that Wilsonian RGE accommodate decoupling of massive particles i.e. corrections from particles with masses greater than Λ are strongly suppressed.

5 Fine-tuning

The standard measure Δ_{c_i} of fine-tuning with respect to the variable c_i is defined as

$$\Delta_{c_i} = \frac{\partial \log v^2}{\partial \log c_i^2}, \quad (5.1)$$

where c_i is a coupling in the model and v is the vacuum expectation value of the field which breaks symmetry spontaneously (here - chiral parity). As a measure of fine-tuning of the whole model we

	coupling					
	ω_Λ	Ω_Λ^2	$g_{3\Lambda}$	λ_Λ	Y_Λ	combined
p	2.24	2.19	2.20	2.20	2.16	2.19
σ	0.05	0.04	0.04	0.04	0.04	0.02

Table 1: Estimated powers p and their standard deviations σ from the fits to the fine-tuning measures (5.1).

take [22, 23],[24]:

$$\Delta = \left(\sum_i \Delta_{c_i}^2 \right)^{\frac{1}{2}}. \quad (5.2)$$

We have computed Δ_{c_i} for parameters of the effective action as functions of scale Λ .

Unfortunately, the effective action for $\Lambda = 0$ cannot be obtained by direct numerical integration of the RGE. The left-hand side of RGE given in Section 3 can be rewritten as

$$\Lambda \frac{dc_i}{d\Lambda} = \frac{dc_i}{d \log (\Lambda/\Lambda_0)}, \quad (5.3)$$

where c_i is a dimensionless parameter and Λ_0 is the scale at which initial conditions are set. From the perspective of numerical integration couplings are functions of $t := \log (\Lambda/\Lambda_0)$. The point $\Lambda = 0$ corresponds to the limit $t \rightarrow -\infty$ which cannot be reached. For that reason we approximated v_Λ for $\Lambda = 0$ (v_0), by the value at $\Lambda = 10^{-4}$ i.e. $v_{10^{-4}}$. We used $\Lambda = 10^{-4}$, because this turns out to be the lowest scale which gives ν_Λ safe from numerical errors. On the other hand, v_Λ changes very slowly between $\Lambda = 1$ and $\Lambda = 10^{-4}$, so $v_{10^{-4}}$ should be a very good approximation for v_0 . To sum up, we have computed fine-tuning measure (5.1) by taking numerical derivatives of ν_Λ with respect to dimensionless parameters ω_Λ , Ω_Λ^2 , $\gamma_{3\Lambda}$, λ_Λ , Y_Λ over the range of scales $10 < \Lambda < 10^6$.

Figs. 14a, 14b, 14c, 14d and 14e show respectively $\left| \frac{\partial \log \nu_{10^{-4}}^2}{\partial \log \omega_\Lambda^2} \right|$, $\left| \frac{\partial \log \nu_{10^{-4}}^2}{\partial \log \Omega_\Lambda^2} \right|$, $\left| \frac{\partial \log \nu_{10^{-4}}^2}{\partial \log \gamma_{3\Lambda}^2} \right|$, $\left| \frac{\partial \log \nu_{10^{-4}}^2}{\partial \log \lambda_\Lambda^2} \right|$ and $\left| \frac{\partial \log \nu_{10^{-4}}^2}{\partial \log Y_\Lambda^2} \right|$.

The spikes visible in Fig. 14 are points where derivatives (5.1) change their signs. Due to logarithmic scale and finite resolution of plots the zeros of derivatives can not be correctly depicted and are represented in Fig. 14 as a finite spikes. Even if one of the derivatives vanishes, the others are typically non-zero and (5.2) stays non-zero and smooth. In Fig. 14f the measure (5.2) as a function of scale Λ is shown. The power function $\propto \Lambda^p$ which has been fitted to fine-tuning curves is shown in red in each plot in the Fig. 14. The fitted powers p are given in Table 1. The power-like functions have been fitted over the interval $10^3 \leq \Lambda \leq 10^6$ (that is above assumed mass thresholds). The reason is the visible change of the behavior of the flow of parameters below 10^3 . On the other hand, the flows above 10^3 can be smoothly extrapolated to arbitrarily high scales.

6 Vacuum stability

An interesting issue is the question of spontaneous symmetry breaking and stability of the potential seen from the point of view of the Wilsonian approach. In this approach one starts with a bare

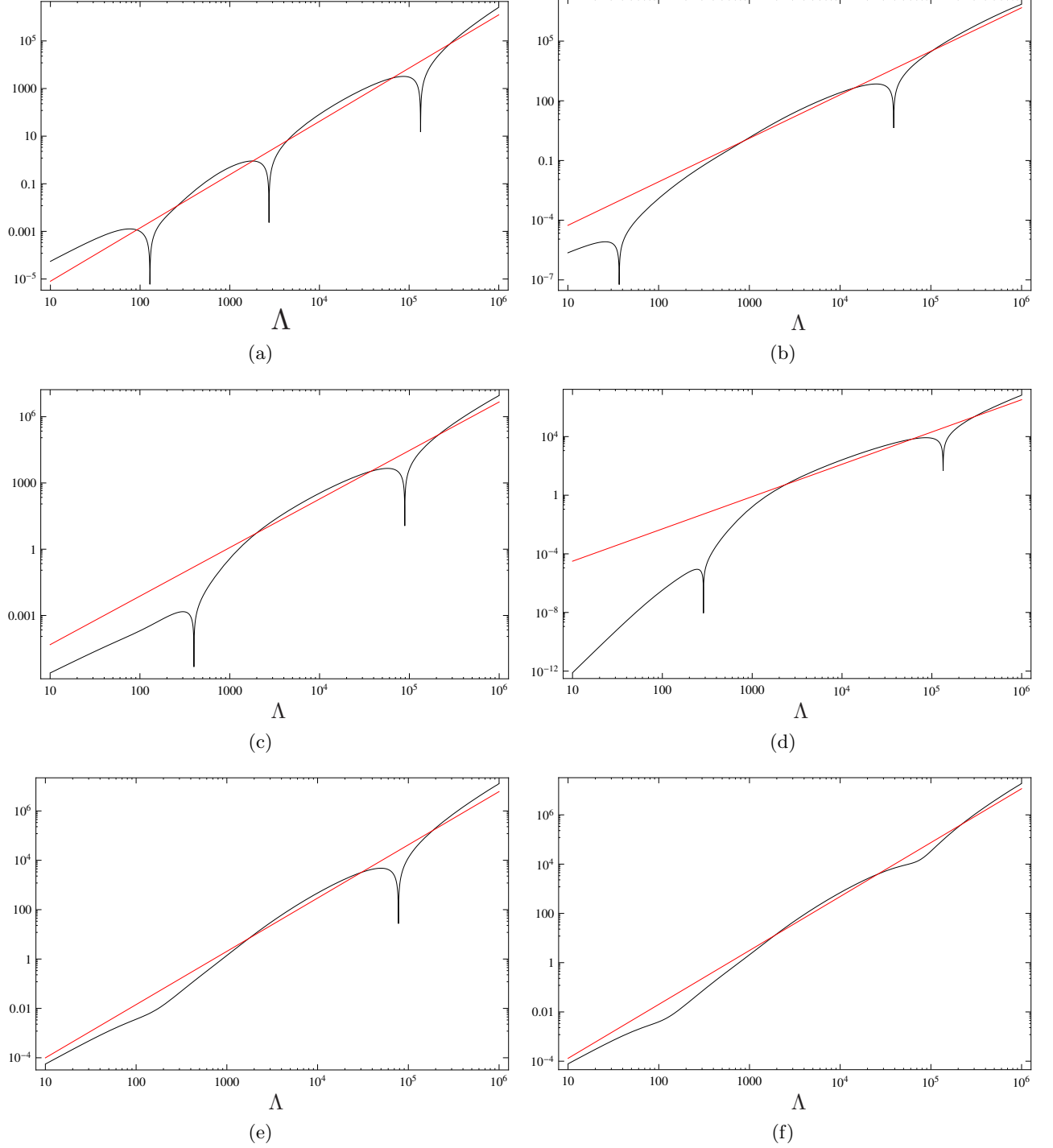


Figure 14: Fine-tuning measures Δ_{c_i} (5.1) for dimensionless parameters: (a)— ω_Λ , (b)— Ω_Λ^2 , (c)— $\gamma_{3\Lambda}$, (d)— λ_Λ and (e)— Y_Λ as functions of Λ in Wilsonian effective action. Combined fine-tuning measure (5.2) is shown in plot (f). Fitted power laws are given as red lines.

action at a high scale and keeps integrating out consecutive shells of momenta, or coarse-graining, to obtain effective action at lower scales. Eventually, the vacuum structure should emerge in the infra-red limit. In the model studied in this paper one can try to answer the question whether the \mathbb{Z}_2 symmetry of (2.1) can be broken by radiative corrections to the scalar mass parameter. What one finds is that for the low values of Ω_Λ^2 and high values of Yukawa coupling Y_Λ in effective action at high Λ , scalar mass-squared parameter can flow to negative value at low values of Λ . The change of sign of M_Λ^2 indicates that stable vacuum of the theory must have non-zero vacuum expectation value of scalar field Φ (as long as the quartic coupling stays positive). Moreover, quartic scalar coupling λ_Λ can run negative for higher Λ which shows similar behavior as the one observed in the Gell-Mann–Low type running (Fig. 13) known from Standard Model. In the context of SM the zero of quartic self-coupling is usually considered as an indication of instability of the electroweak vacuum and of the existence of a second minimum of the scalar potential. In the Wilsonian approach however, simple analysis based on quartic coupling alone is insufficient, because higher dimension operators with higher powers of the scalar field Φ , which we suppressed in our truncation (2.3), may dominate scalar potential for large values of Φ . The impact coming from higher dimension operators was previously investigated in [25] and [26]. To draw stronger conclusions one needs a procedure of resummation of possibly large contributions to scalar potential coming from operators with all higher powers of Φ . However, the observed instability of Wilsonian quartic coupling may be seen as an indication of a crossover behavior at higher scales, since in the region of $\langle\Phi\rangle$ comparable to Λ and well below the UV cutoff, one still expects higher-dimension operators to be suppressed with respect to the quartic one by powers of small couplings, since well below the UV cutoff the coefficients of higher-order operators should be dominated by "renormalizable" couplings.

The example of a solution demonstrating such features is plotted in the Fig. 15. For this solution scalar mass parameter Ω_Λ^2 vanishes at the scale $\Lambda = 2.67 \times 10^4$ and quartic coupling λ_Λ has a zero at $\Lambda = 1.07 \times 10^6$. While investigating features of this solution one can notice a strong dependence of the scale of symmetry breaking on the value of Yukawa coupling Y_Λ . This fine-tuning problem makes one choose very precisely the initial condition for Yukawa coupling in order to make the symmetry breaking scale low.

The issue of spontaneous symmetry breaking can be studied with the help of the Fig. 16 in which numerical solutions with different initial conditions are projected on the plane spanned by λ_Λ and Ω_Λ^2 . All solutions given there have $Y_\Lambda = 1.461$, $\lambda_\Lambda = 0.1$ and $v_\Lambda = g_{3\Lambda} = m_\Lambda = 0$ as a initial conditions set at $\Lambda = 10^6$, but initial value of Ω_Λ^2 varying. From Fig. 16 one can see that if for any scale Λ couplings will be lower than certain critical value Ω_{cr}^2 , then Ω^2 will run negative in the IR and chiral parity will be spontaneously broken. Moreover as can be seen in the Fig. 17 critical value Ω_{cr}^2 is rather sensitive to Yukawa coupling Y . From the behavior shown in the Fig. 17 one concludes that Ω_{cr}^2 decreases when the value of Y increases and for any value of Ω^2 there exist a critical value of Yukawa coupling Y_{cr} . Once Y_{cr} is exceeded, the radiative spontaneous symmetry breaking appears. Hence fourth quadrant of the Fig. 17 gives direct evidence of the Coleman–Weinberg mechanism at work.

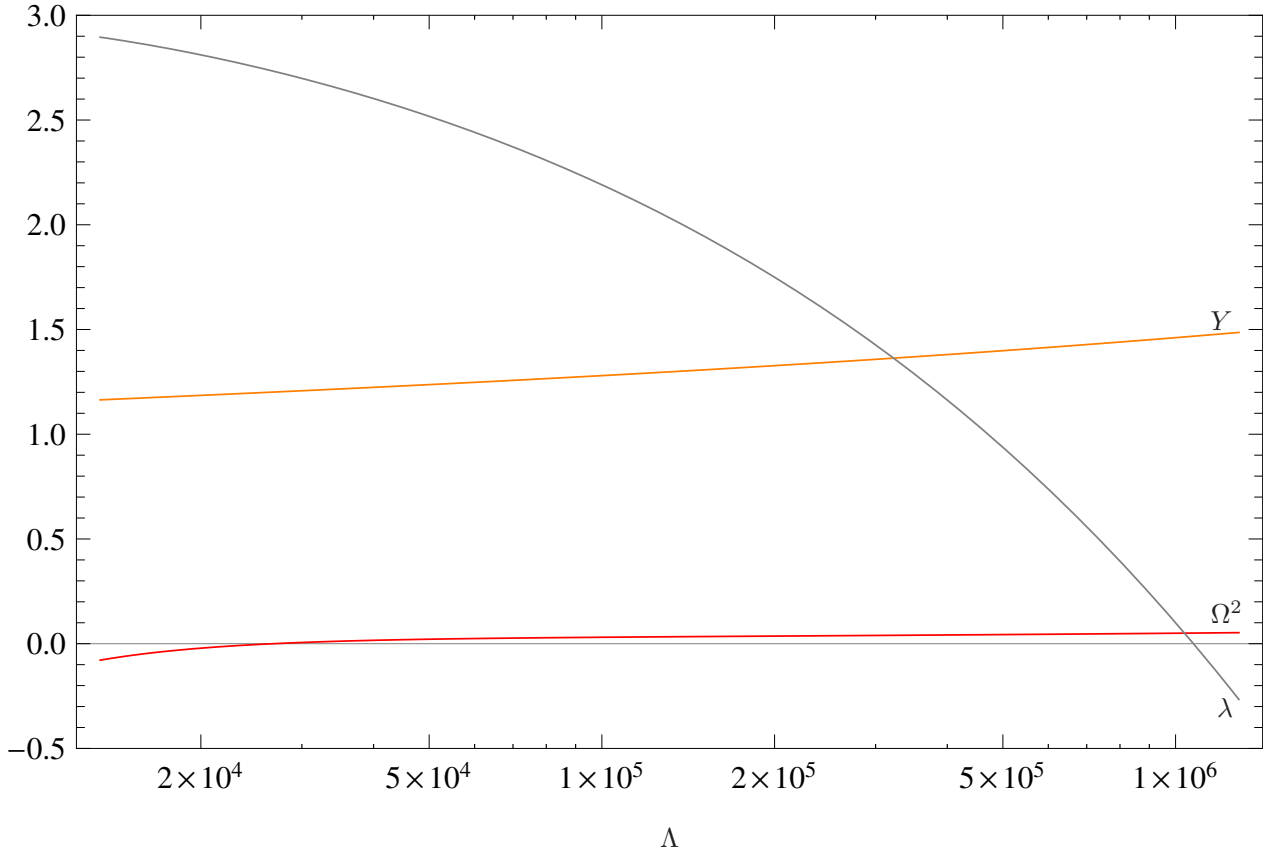


Figure 15: Example of numerical solution of RGE in which radiative symmetry breaking takes place. Plot corresponds to values $Y_\Lambda = 1.461$, $M_\Lambda^2 = 5 \times 10^{10}$, $\lambda_\Lambda = 0.1$ and $v_\Lambda = g_{3\Lambda} = m_\Lambda = 0$ at $\Lambda = 10^6$.

7 Conclusions

In this paper we have used Wilsonian effective action to investigate fine-tuning and vacuum stability in a simple model exhibiting spontaneous breaking of a discrete symmetry and large fermionic radiative corrections which are able to destabilize quartic scalar self-coupling. Regulator independence of Wilsonian RG provides consistent and well-defined procedure to analyze the issue of quadratic divergences. In the simplified model simulating certain features of SM the Wilsonian renormalization group equations have been studied. We have explained in what sense the truncation adopted in the calculations corresponds to 1-loop Gell-Mann–Low running. In fact, in both cases the approximations used correspond to lowest-order quantum effects within each renormalization scheme.

Numerical solutions of RGE have revealed interesting behavior, caused by the same diagrams that generate quadratic divergences. An operator relevant near Gaussian fixed point (for example mass parameter for scalar particles) can run like marginal or even irrelevant operator, rather than decrease with growing scale. Furthermore solutions for different physical quantities flow close to each other with increasing scale. The flow in the direction of some common value indicates severe

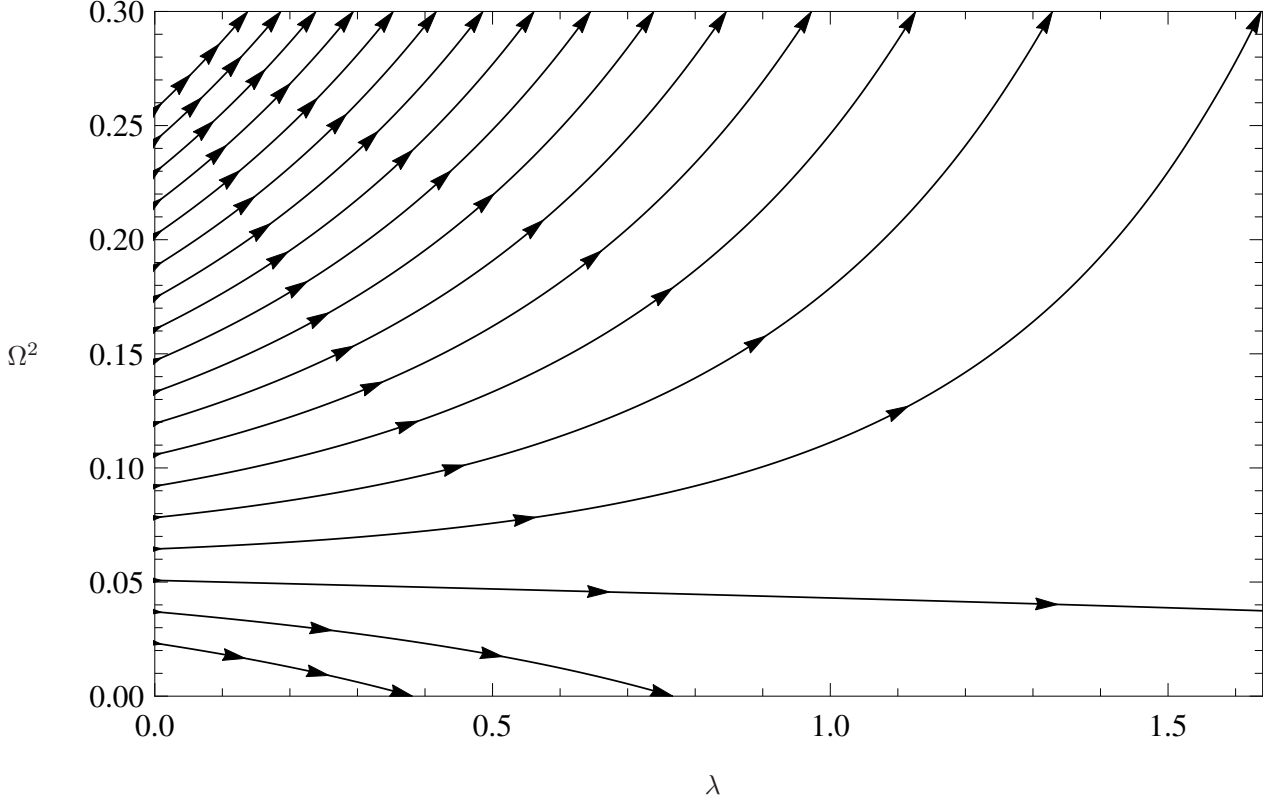


Figure 16: Flow of λ_Λ and Ω_Λ^2 in the range of parameters where spontaneous symmetry breaking takes place. Plot corresponds to $Y_\Lambda = 1.461$, $\lambda_\Lambda = 0.1$, $v_\Lambda = g_{3\Lambda} = m_\Lambda = 0$ and varying M_Λ^2 at $\Lambda = 10^6$. Moving along the lines in the direction of arrows corresponds to decreasing scale Λ .

fine-tuning. In such a situation small changes of boundary values of parameters at the high scale produce very different vacuum expectation values for scalar field and other measurable quantities at low energies. We have estimated fine-tuning as a function of scale of the effective theory. For all parameters the adopted measure of fine-tuning grows rapidly. Power-like functions fitted to the obtained fine-tuning curves grow faster than Λ^2 over the range of scales taken into account in the study.

It should be stressed that Wilsonian RGE, in contrast to Gell-Mann–Low running, accommodate automatically decoupling of heavy particles. As noticed in Section 4, the contribution to flow coming from particles with masses M_{heavy} greater than the scale Λ of the effective action is strongly suppressed. The main contributions to the interactions generated by heavy states are integrated out during calculation of the effective action for $\Lambda \ll M_{heavy}$ and are included in the effective Wilson coefficients. These properties of Wilsonian RGE explain why fine-tuning of Wilson parameters is so interesting. Let us imagine a more fundamental theory (say theory A) in which the SM is embedded. If one calculates in theory A the effective action for the scale Λ below, but not very much, the lowest mass of the particles from the New Physics sector, one obtains certain values of the Wilson coefficients c^A . On the other hand one can extrapolate the flow obtained from the SM to the

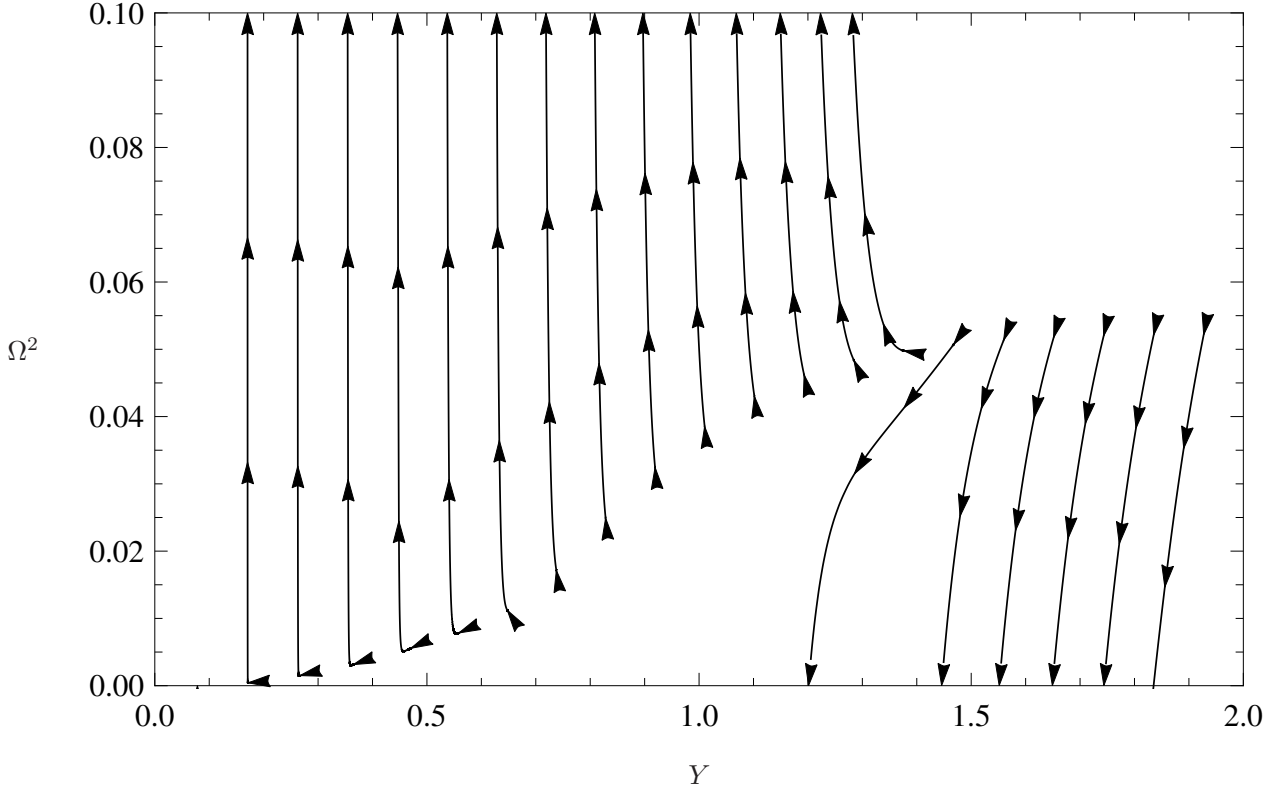


Figure 17: Flow of Y_Λ and Ω_Λ^2 in the range of parameters where spontaneous symmetry breaking takes place. Plot corresponds to $\lambda_\Lambda = 0.1$, $M_\Lambda^2 = 5 \times 10^{10}$, $v_\Lambda = g_{3\Lambda} = m_\Lambda = 0$ and varying Y_Λ at $\Lambda = 10^6$. Moving along the lines in the direction of arrows corresponds to decreasing scale Λ .

scale Λ and calculate the Wilson coefficients c^{SM} . Couplings computed in both ways should match, that is $c_\Lambda^A = c_\Lambda^{SM}$. If the couplings c^A are different from c^{SM} at the level of fine-tuning Δc , that is $c_\Lambda^A(1 \pm \Delta c) = c_\Lambda^{SM}$, theory A will produce IR effective action completely different from the SM.

We have studied the issue of spontaneous symmetry breaking due to radiative corrections in the Wilsonian framework. We have demonstrated that there exists a critical value Ω_{cr}^2 below which Ω^2 runs negative in the IR and symmetry becomes spontaneously broken. Moreover, critical value Ω_{cr}^2 is sensitive to Yukawa coupling Y . One can see that Ω_{cr}^2 decreases when the value of Y increases and for any value of Ω^2 there exist a critical value of Yukawa coupling Y_{cr} . Once Y_{cr} is exceeded, the radiative spontaneous symmetry breaking appears, which is a direct evidence of the Coleman–Weinberg mechanism at work.

Acknowledgements

This work has been supported by National Science Center under research grant DEC-2012/04/A/ST2/00099 and partially under research grant DEC-2011/01/M/ST2/02466. Authors (Z.L.) are grateful to the Mainz Institute for Theoretical Physics (MITP) for its hospitality and its partial support during the completion of this work.

A Wilsonian RGE

The aim of this section is to present brief introduction to the methods of Wilsonian RGE and to set the notation. We will define most of the terms that we used in the text of this paper. Method of discrete Renormalization Group Equations has been presented in Wilson's and Kogut's review [27], a short introduction can be found in book of Peskin and Schroeder [28]. RGE for Legendre effective action have been derived in [29, 30, 31]. Interesting formal developments on FRG are presented in [32]. Introductory review on FRG in gauge theories has been given in [33]. Further references can be found in the book [34] as well as in [35] and [36].

A.1 Wilsonian effective action

The fundamental object of QFT is generating functional $\mathcal{Z}[J]$ which is given in path integral formalism by formal expression²

$$\mathcal{Z}[J] = \int \mathcal{D}\Phi e^{-S_E[\Phi] + \int d^4x_E J\Phi} \quad (\text{A.1})$$

where S_E is Euclidean action for the Φ field(s) and J is source(s). We can rewrite (A.1) in equivalent form (A.2) using Fourier transform³ $\hat{\Phi}$

$$\mathcal{Z}[\hat{J}] = \int \mathcal{D}\hat{\Phi} e^{-S_E[\hat{\Phi}] + \int \frac{d^4p}{(2\pi)^4} \hat{J}\hat{\Phi}} = \int \prod_p d\hat{\Phi}(p) e^{-S_E[\hat{\Phi}(p)] + \int \frac{d^4p}{(2\pi)^4} \hat{J}(p)\hat{\Phi}(p)}. \quad (\text{A.2})$$

We introduce projection operator

$$\left(b_\Lambda \hat{F}\right)(p) = \theta_0(p^2 - \Lambda^2) \hat{F}(p), \quad (\text{A.3})$$

where θ_0 is defined as follows

$$\theta_0(x) = \begin{cases} 1 & \text{for } x > 0 \\ 0 & \text{for } x \leq 0 \end{cases}. \quad (\text{A.4})$$

We can divide integration variables $\hat{\Phi}(p)$ into two classes:

$$\hat{\Phi}_{\leq}(p) = (1 - b_\Lambda) \hat{\Phi}(p), \quad \hat{\Phi}_{>}(p) = b_\Lambda \hat{\Phi}(p). \quad (\text{A.5})$$

It is easy to find that

$$\prod_p d\hat{\Phi}(p) = \left(\prod_{p: p^2 \leq \Lambda^2} d\hat{\Phi}_{\leq}(p) \right) \left(\prod_{p': p'^2 > \Lambda^2} d\hat{\Phi}_{>}(p') \right). \quad (\text{A.6})$$

Action $S_E[\hat{\Phi}]$ can be rewritten as

$$S_E[\hat{\Phi}_{\leq} + \hat{\Phi}_{>}] = S_E[\hat{\Phi}_{\leq}] + S_E[\hat{\Phi}_{>}] + \mathcal{S}_E[\hat{\Phi}_{\leq}, \hat{\Phi}_{>}] \quad (\text{A.7})$$

²It is convenient to use Euclidean space in the context of Wilsonian RGE, so we will assume for a moment that we use Euclidean formulation of QFT.

³We will denote Fourier transform of field $F(x)$ as $\hat{F}(p)$.

where we denoted by $\mathcal{S}_E[\hat{\Phi}_\leq, \hat{\Phi}_>]$ the part which depends on both $\hat{\Phi}_\leq$ and $\hat{\Phi}_>$. In this notation generating functional $\mathcal{Z}[\hat{J}]$ takes form

$$\begin{aligned} \mathcal{Z}[\hat{J}_\leq, \hat{J}_>] = & \int \prod_{p: p^2 \leq \Lambda^2} d\hat{\Phi}_\leq(p) e^{-S_E[\hat{\Phi}_\leq(p)] + \int \frac{d^4 p}{(2\pi)^4} \hat{J}_\leq(p) \hat{\Phi}_\leq(p)} \\ & \cdot \int \prod_{p': p'^2 > \Lambda^2} d\hat{\Phi}_>(p') e^{-S_E[\hat{\Phi}_>(p')] - S_E[\hat{\Phi}_\leq(p), \hat{\Phi}_>(p')] + \int \frac{d^4 p}{(2\pi)^4} \hat{J}_>(p') \hat{\Phi}_>(p')} \end{aligned} \quad (\text{A.8})$$

where we have used orthogonality of modes with different momenta and have defined

$$\hat{J}_\leq(p) = (1 - b_\Lambda) \hat{J}(p), \quad \hat{J}_>(p) = b_\Lambda \hat{J}(p). \quad (\text{A.9})$$

Let us now imagine for a moment that we integrate over all $\hat{\Phi}_>$ in generating functional $\mathcal{Z}[\hat{J}_\leq, \hat{J}_>]$. Then we will obtain

$$\mathcal{Z}[\hat{J}_\leq, \hat{J}_>] = \int \prod_{p: p^2 \leq \Lambda^2} d\hat{\Phi}_\leq(p) e^{-S_E[\hat{\Phi}_\leq] + \int \frac{d^4 p}{(2\pi)^4} \hat{J}_\leq(p) \hat{\Phi}_\leq(p)} \mathcal{Z}_>[\hat{J}_>]. \quad (\text{A.10})$$

If we restricts ourselves to generating functional $\mathcal{Z}_\leq[\hat{J}_\leq]$ for Greens functions of low-energy modes $\hat{\Phi}_\leq$ then it will get form:

$$\mathcal{Z}_\leq[\hat{J}_\leq] = \int \prod_{p: p^2 \leq \Lambda^2} d\hat{\Phi}_\leq(p) e^{-S_E[\hat{\Phi}_\leq] + \log \mathcal{Z}_>[0] + \int \frac{d^4 p}{(2\pi)^4} \hat{J}_\leq(p) \hat{\Phi}_\leq(p)}. \quad (\text{A.11})$$

Action $S_\Lambda[\hat{\Phi}_\leq] := S_E[\hat{\Phi}_\leq] - \log \mathcal{Z}_>[0]$ is called Wilsonian effective action for scale Λ .

A.2 Flow equations

We define generating functional $W_\Lambda[\hat{J}]$ by equation

$$e^{W_\Lambda[\hat{J}]} := \int \prod_{p: p^2 > \Lambda^2} d\hat{\Phi}_>(p) e^{-S_E[\hat{\Phi}_\leq + \hat{\Phi}_>] + \int \frac{d^4 p}{(2\pi)^4} \hat{J}(p) (\hat{\Phi}_\leq(p) + \hat{\Phi}_>(p))}. \quad (\text{A.12})$$

If S_E can be decomposed as

$$S_E[\hat{\varphi}] =: S_I[\hat{\varphi}] + S_G[\hat{\varphi}] \quad (\text{A.13})$$

with some arbitrary interaction part S_I , and a Gaussian part of the general form

$$S_G[\hat{\varphi}] =: - \int \frac{d^4 p}{(2\pi)^4} \frac{1}{2} \hat{\varphi}(-p) G^{-1}(p) \hat{\varphi}(p). \quad (\text{A.14})$$

then it can be showed that following definition

$$e^{W_\Lambda[\hat{J}]} = \int \prod_p d\hat{\Phi}(p) e^{-S_I[\hat{\Phi}(p)] + \int \frac{d^4 p}{(2\pi)^4} [\frac{1}{2} \hat{\Phi}(-p) \theta_0(p^2 - \Lambda^2) G^{-1}(p) \hat{\Phi}(p) + \hat{J}(p) \hat{\Phi}(p)]}. \quad (\text{A.15})$$

is equivalent to (A.12).

For calculating β -functions, it is convenient to consider Legendre transform $\Gamma_\Lambda[\phi]$ of generating functional $W_\Lambda[J]$. Before we define Wilsonian RGE we should reduce redundant degrees of freedom in $\Gamma_\Lambda[\phi]$. Firstly it can happen that

$$\left. \frac{\delta \Gamma_\Lambda}{\delta \phi} \right|_{\phi=0} \neq 0. \quad (\text{A.16})$$

In such a case we shift the the field $\phi \rightarrow \phi_0 + \varphi$ by the solution ϕ_0 of equation $\left. \frac{\delta \Gamma_\Lambda}{\delta \phi} \right|_{\phi=\phi_0} = 0$. Secondly there are redundant degree of freedom corresponding to the rescaling of the field φ . We assume that φ has canonical kinetic term in $\Gamma_\Lambda[\varphi]$. RGE are differential equations describing change of $\Gamma_\Lambda[\varphi]$ due to the change of scale Λ .

Legendre effective action $\Gamma_\Lambda[\varphi]$ can be expanded in Taylor series in powers of field φ

$$\Gamma_\Lambda[\varphi] = \sum_{n \in \mathbb{N}} \frac{1}{n!} \hat{\varphi}^n \frac{\delta^n}{\delta \hat{\varphi}^n} \Gamma_\Lambda. \quad (\text{A.17})$$

Each coefficient of Taylor expansion can be expanded in derivatives of φ

$$\frac{\delta}{\delta \hat{\varphi}(p_1)} \cdots \frac{\delta}{\delta \hat{\varphi}(p_n)} \Gamma_\Lambda = \left(\prod_{i=1}^n \int \frac{d^4 p_i}{(2\pi)^4} \right) \delta \left(\sum_{i=1}^n p_i \right) \sum_{i_1, \dots, i_n \in \mathbb{N}} C_{i_1, \dots, i_n}^{(n)} p_1^{i_1} \cdots p_n^{i_n}. \quad (\text{A.18})$$

Coefficients $C_i^{(n)}$ are called Wilson coefficients. It is convenient to use dimensionless parameters

$$c_i^{(n)} = C_i^{(n)} \Lambda^{-\dim C_i^{(n)}} \quad (\text{A.19})$$

where $\dim C_i^{(n)}$ is canonical dimension of the coefficient. RGE expressed in terms of dimensionless parameters is dynamical system.

Legendre effective action $\Gamma_\Lambda[\varphi]$ in the limit $\Lambda \rightarrow \infty$ is called classical action. This limit usually does not exist in strict mathematical sense, because Wilson coefficients are typically divergent when $\Lambda \rightarrow \infty$. Classical action for theories that are not finite should be thought as a formal expression which must be renormalized.

A.3 Perturbation theory

Wilsonian effective action and flow equations can be approximately derived in perturbation theory and expressed by Feynman diagrams. Starting with (A.15) the Wilsonian effective action $W_\Lambda[\hat{J}]$ (so Legendre effective action $\Gamma_\Lambda[\varphi]$ too) can be computed in perturbation theory in a manner analogous to computation of the generating functional for connected Green's functions $W[\hat{J}]$ (1PI effective action $\Gamma_{1\text{PI}}[\varphi]$), but with a propagator substituted by a propagator with a cutoff:

$$G_\Lambda(p) := \theta_0(p^2 - \Lambda^2)G(p). \quad (\text{A.20})$$

Legendre effective action $\Gamma_\Lambda[\varphi]$, like the 1PI effective action $\Gamma_{1\text{PI}}[\varphi]$, has usually infinitely many terms. Wilsonian RGE for a generic theory is the set of infinitely many coupled equations for infinitely many couplings which rarely can be solved exactly. For practical purposes one typically have to use certain approximation strategy. The most common consists in truncation of effective action and in considering only a subset of Wilson coefficients which are relevant for the problem in question.

B Derivatives of loop integrals with IR cutoff

During calculation of RGE we used following derivatives of integrals $I_N(R)$ defined in [17].

$$\frac{\partial}{\partial \Lambda} I_1(R) = \Lambda^2 \frac{1}{\Lambda} \frac{-2i}{(4\pi)^2} \frac{1}{1 + \frac{R}{\Lambda^2}} + \mathcal{O}(\varepsilon) \quad (\text{B.1})$$

$$\frac{\partial}{\partial \Lambda} I_2(R) = \frac{1}{\Lambda} \frac{-2i}{(4\pi)^2} \frac{1}{(1 + \frac{R}{\Lambda^2})^2} + \mathcal{O}(\varepsilon) \quad (\text{B.2})$$

$$\frac{\partial}{\partial \Lambda} I_N(R) = \Lambda^{-2(N-2)} \frac{1}{\Lambda} \frac{-2i}{(4\pi)^2} \frac{1}{(1 + \frac{R}{\Lambda^2})^N} + \mathcal{O}(\varepsilon) \quad (\text{B.3})$$

C 1-loop matching conditions

We used FeynArts/FeynCalc packages for Mathematica to calculate 1-loop matching conditions in order to express Wilson coefficients of effective action on matching scale Λ by physical quantities. In addition we used ANT package modified to be compatible with FeynCalc. Moreover, we added infinite terms listed in [21] to the expressions in this package in order to check consistency of our calculation. We have written an analogous package that contains loop integrals in dimensional regularization with IR cutoff.

We expressed parameters of the effective action in terms of physical vacuum expectation value v_{ph} of Φ field, pole masses m_{ph} , M_{ph} of respectively Ψ and Φ fields. We have defined Yukawa coupling Y_{ph} and trilinear coupling g_{3ph} as a 1PI part of scattering amplitude at kinematic point with incoming momentum square equal to μ^2 and outgoing momenta squares equal to μ^2 and 0. In definition of Y_{ph} we assumed that outgoing fermion has non-zero momentum. Coupling λ_{ph} is defined at kinematic point with Mandelstam variables equal to μ^2 .

Diagrams that contribute to matching conditions are discussed in Section 3 and are presented at Figs. from 5 to 10. The matching conditions obtained this way are of the following form:

$$\begin{aligned} v_\Lambda = v_{ph} &+ \frac{1}{2} \frac{g_{3ph}}{(4\pi)^2 M_{ph}^2} \left(\Lambda^2 - M_{ph}^2 \log \left(\frac{\Lambda^2}{M_{ph}^2} + 1 \right) \right) \\ &- 4 \frac{Y_{ph}}{(4\pi)^2 M_{ph}^2} \left(\Lambda^2 m_{ph} - m_{ph}^3 \log \left(\frac{\Lambda^2}{m_{ph}^2} + 1 \right) \right) \\ &- \frac{v_{ph}}{2} \left[\frac{2}{3} \frac{Y_{ph}^2}{(4\pi)^2} \left(\frac{M_{ph}^2}{m_{ph}^2} - \frac{\Lambda^2 (5\Lambda^2 + 11m_{ph}^2)}{(\Lambda^2 + m_{ph}^2)^2} + 3 \log \left(\frac{\Lambda^2}{m_{ph}^2} + 1 \right) \right) \right. \\ &\quad \left. + \frac{1}{12} \frac{g_{3ph}^2}{(4\pi)^2} \left(\frac{3\Lambda^2}{(\Lambda^2 + M_{ph}^2)^2} - \frac{1}{\Lambda^2 + M_{ph}^2} + \frac{1}{M_{ph}^2} \right) \right] \quad (\text{C.1}) \end{aligned}$$

$$\begin{aligned}
m_\Lambda = m_{ph} - \frac{1}{6} \frac{Y_{ph}^2}{(4\pi)^2} & \left[\log \left(\frac{\Lambda^2}{m_{ph}^2} + 1 \right) \left(\frac{6m_{ph}^3}{M_{ph}^2 - m_{ph}^2} - \frac{3(m_{ph}^5 - \Lambda^4 m_{ph})}{(M_{ph}^2 - m_{ph}^2)^2} \right) \right. \\
& + \log \left(\frac{\Lambda^2}{M_{ph}^2} + 1 \right) \left(\frac{3(m_{ph}^5 - \Lambda^4 m_{ph})}{(M_{ph}^2 - m_{ph}^2)^2} - \frac{6m_{ph}^3}{M_{ph}^2 - m_{ph}^2} - 9m_{ph} \right) \\
& + \log \left(\frac{M_{ph}^2}{m_{ph}^2} \right) \left(-\frac{3\Lambda^4 m_{ph}}{(M_{ph}^2 - m_{ph}^2)^2} + \frac{6m_{ph}^9}{(M_{ph}^2 - m_{ph}^2)^4} + \frac{12m_{ph}^7}{(M_{ph}^2 - m_{ph}^2)^3} \right) \\
& \left. + \frac{3\Lambda^2 m_{ph} + 4m_{ph}^3}{M_{ph}^2 - m_{ph}^2} - \frac{6m_{ph}^7}{(M_{ph}^2 - m_{ph}^2)^3} - \frac{9m_{ph}^5}{(M_{ph}^2 - m_{ph}^2)^2} - \frac{4m_{ph}^3}{M_{ph}^2} \right] \quad (C.2)
\end{aligned}$$

$$\begin{aligned}
M_\Lambda^2 = M_{ph}^2 - \frac{1}{2} \frac{\lambda_{ph}}{(4\pi)^2} & \left[\Lambda^2 - M_{ph}^2 \log \left(\frac{\Lambda^2}{M_{ph}^2} + 1 \right) \right] \\
& + \frac{1}{12} \frac{g_{3ph}^2}{(4\pi)^2} \left[-\frac{2\Lambda^2}{M_{ph}^2 + \Lambda^2} + 6 \log \left(\frac{\Lambda^2}{M_{ph}^2} + 1 \right) - \frac{3\Lambda^4}{(M_{ph}^2 + \Lambda^2)^2} \right] \\
& + \frac{1}{3} \frac{Y_{ph}^2}{(4\pi)^2} \left[(6M_{ph}^2 - 36m_{ph}^2) \log \left(\frac{\Lambda^2}{m_{ph}^2} + 1 \right) \right. \\
& \left. + \frac{-2\Lambda^2 M_{ph}^2 (5\Lambda^2 + 11m_{ph}^2)}{(m_{ph}^2 + \Lambda^2)^2} + \frac{M_{ph}^4}{m_{ph}^2} + \frac{12\Lambda^2 (3m_{ph}^2 + \Lambda^2)}{m_{ph}^2 + \Lambda^2} \right] \quad (C.3)
\end{aligned}$$

$$\begin{aligned}
g_{3\Lambda} = g_{3ph} - \frac{1}{6} \frac{g_{3ph}\lambda_{ph}}{(4\pi)^2} & \left[-9 \log \left(\frac{\Lambda^2}{M_{ph}^2} + 1 \right) - \frac{2\mu^2}{M_{ph}^2} + \frac{9\Lambda^2}{M_{ph}^2 + \Lambda^2} \right] \\
& - \frac{1}{24} \frac{g_{3ph}^3}{(4\pi)^2} \left[\frac{4\mu^2}{M_{ph}^4} - \frac{15\Lambda^2}{(M_{ph}^2 + \Lambda^2)^2} - \frac{3}{M_{ph}^2 + \Lambda^2} + \frac{9}{M_{ph}^2} \right] \\
& - \frac{4}{3} \frac{Y_{ph}^3}{(4\pi)^2} \left[9m_{ph} \log \left(\frac{\Lambda^2}{m_{ph}^2} + 1 \right) + \frac{\mu^4}{m_{ph}^3} + \frac{3\mu^2}{m_{ph}} - \frac{9\Lambda^2 m_{ph}}{m_{ph}^2 + \Lambda^2} \right. \\
& \quad \left. - \frac{3\Lambda^4 m_{ph}}{(m_{ph}^2 + \Lambda^2)^2} - 3m_{ph} \right] \\
& - \frac{1}{2} \frac{\lambda_{ph}}{(4\pi)^2} \left(\Lambda^2 - M_{ph}^2 \log \left(\frac{\Lambda^2}{M_{ph}^2} + 1 \right) \right) \\
& + \frac{g_{3ph} Y_{ph}^2}{(4\pi)^2} \left[3 \log \left(\frac{\Lambda^2}{m_{ph}^2} + 1 \right) + \frac{M_{ph}^2}{m_{ph}^2} - \frac{\Lambda^2 (5\Lambda^2 + 11m_{ph}^2)}{(m_{ph}^2 + \Lambda^2)^2} \right] \quad (C.4)
\end{aligned}$$

$$\begin{aligned}
\lambda_\Lambda = \lambda_{ph} - \frac{1}{24} \frac{g_{3ph}^2 \lambda_{ph}}{(4\pi)^2} & \left[-\frac{15\mu^2}{M_{ph}^4} - \frac{48\Lambda^2}{(M_{ph}^2 + \Lambda^2)^2} - \frac{32}{M_{ph}^2 + \Lambda^2} + \frac{68}{M_{ph}^2} \right] \\
& + \frac{1}{2} \frac{g_{3ph}^4}{(4\pi)^2} \left[-\frac{2\Lambda^2}{(M_{ph}^2 + \Lambda^2)^3} - \frac{1}{(M_{ph}^2 + \Lambda^2)^2} + \frac{1}{M_{ph}^4} \right] \\
& - \frac{1}{2} \frac{Y_{ph}^4}{(4\pi)^2} \left[48 \log \left(\frac{\Lambda^2}{m_{ph}^2} + 1 \right) + \frac{9\mu^4}{m_{ph}^4} + \frac{44\mu^2}{m_{ph}^2} - \frac{48\Lambda^2}{m_{ph}^2 + \Lambda^2} \right. \\
& \quad \left. - \frac{128\Lambda^6}{(m_{ph}^2 + \Lambda^2)^3} + \frac{96\Lambda^4}{(m_{ph}^2 + \Lambda^2)^2} - 96 \right] \\
& - \frac{1}{4} \frac{\lambda_{ph}^2}{(4\pi)^2} \left[-6 \log \left(\frac{\Lambda^2}{M_{ph}^2} + 1 \right) + \frac{\mu^2}{M_{ph}^2} + \frac{6\Lambda^2}{M_{ph}^2 + \Lambda^2} \right] \\
& + \frac{4}{3} \frac{Y_{ph}^2 \lambda_{ph}}{(4\pi)^2} \left[3 \log \left(\frac{\Lambda^2}{m_{ph}^2} + 1 \right) + \frac{M_{ph}^2}{m_{ph}^2} - \frac{\Lambda^2 (5\Lambda^2 + 11m_{ph}^2)}{(m_{ph}^2 + \Lambda^2)^2} \right] \quad (C.5)
\end{aligned}$$

$$\begin{aligned}
Y_\mu = Y_{ph} - \frac{1}{36} \frac{Y_{ph}^3}{(4\pi)^2} & \left[\log \left(\frac{\Lambda^2}{M_{ph}^2} + 1 \right) \left(-\frac{18(m_{ph}^4 + \Lambda^4)}{(M_{ph}^2 - m_{ph}^2)^2} - \frac{72m_{ph}^2}{M_{ph}^2 - m_{ph}^2} - 54 \right) \right. \\
& + \log \left(\frac{\Lambda^2}{m_{ph}^2} + 1 \right) \left(\frac{18(m_{ph}^4 + \Lambda^4)}{(M_{ph}^2 - m_{ph}^2)^2} + \frac{72m_{ph}^2}{M_{ph}^2 - m_{ph}^2} - 36 \right) \\
& + \log \left(\frac{M_{ph}^2}{m_{ph}^2} \right) \left(\frac{36(-5\mu^4 m_{ph}^4 - \mu^2 m_{ph}^6 + 3m_{ph}^8)}{(M_{ph}^2 - m_{ph}^2)^4} - \frac{18(4\mu^4 m_{ph}^2 - 3\mu^2 m_{ph}^4 - 6m_{ph}^6)}{(M_{ph}^2 - m_{ph}^2)^3} \right. \\
& + \frac{18(2m_{ph}^2 - \mu^2)}{M_{ph}^2 - m_{ph}^2} - \frac{6(10\mu^2 m_{ph}^2 + 6m_{ph}^4 + 3\Lambda^4)}{(M_{ph}^2 - m_{ph}^2)^2} - \frac{12(9\mu^4 m_{ph}^6 + 8\mu^2 m_{ph}^8)}{(M_{ph}^2 - m_{ph}^2)^5} \Big) \\
& + \frac{12\Lambda^2(5\Lambda^2 + 11m_{ph}^2)}{(\Lambda^2 + m_{ph}^2)^2} + \frac{27M_{ph}(m_{ph} + M_{ph})(-\mu^4 + 6\mu^2 m_{ph}^2 + 6m_{ph}^4)}{2(m_{ph}^2 - M_{ph}^2)^3} \\
& - \frac{18(\mu^2 + 3m_{ph}^2)}{M_{ph}^2} + \frac{(m_{ph}^2 + M_{ph}^2)(-9\mu^4 + 29\mu^2 m_{ph}^2 + 27m_{ph}^4)}{4(m_{ph}^2 - M_{ph}^2)^2} \\
& + \frac{3(m_{ph}^4 + 6m_{ph}^2 M_{ph}^2 + M_{ph}^4)(9\mu^2 + 8m_{ph}^2)}{4(m_{ph}^2 - M_{ph}^2)^4} - \frac{12M_{ph}^2}{m_{ph}^2} \\
& \left. - \frac{(m_{ph}^4(121\mu^2 + 45\Lambda^2) + m_{ph}^2(3\mu^4 + 36\Lambda^4 + 121\mu^2\Lambda^2) + 81m_{ph}^6 + 3\mu^4\Lambda^2)}{2m_{ph}^2(m_{ph}^2 - M_{ph}^2)(m_{ph}^2 + \Lambda^2)} \right] \\
& - \frac{1}{36} \frac{g_{3ph} Y_{ph}^2}{(4\pi)^2} \left[18 \left(\log \left(\frac{\Lambda^2}{M_{ph}^2} + 1 \right) - \log \left(\frac{\Lambda^2}{m_{ph}^2} + 1 \right) \right) \frac{m_{ph}^3}{(m_{ph}^2 - M_{ph}^2)^2} \right. \\
& + \log \left(\frac{M_{ph}^2}{m_{ph}^2} \right) \left(\frac{48\mu^2 m_{ph}^7}{(M_{ph}^2 - m_{ph}^2)^5} + \frac{18\mu^2 m_{ph}^5}{(M_{ph}^2 - m_{ph}^2)^4} + \frac{36(m_{ph}^5 - \mu^2 m_{ph}^3)}{(M_{ph}^2 - m_{ph}^2)^3} - \frac{18m_{ph}^3}{(M_{ph}^2 - m_{ph}^2)^2} \right) \\
& - \frac{48\mu^2 m_{ph}^5}{(M_{ph}^2 - m_{ph}^2)^4} + \frac{6\mu^2 m_{ph}^3}{(M_{ph}^2 - m_{ph}^2)^3} - \frac{m_{ph}(36m_{ph}^2 - 29\mu^2)}{(M_{ph}^2 - m_{ph}^2)^2} - \frac{18\Lambda^2 m_{ph}}{(m_{ph}^2 + \Lambda^2)(M_{ph}^2 + \Lambda^2)} \\
& + \frac{12\mu^2}{m_{ph} M_{ph}^2} + \frac{6(-2\mu^2 m_{ph}^2 + 9\Lambda^2 m_{ph}^2 + 6m_{ph}^4 - 2\mu^2 \Lambda^2)}{m_{ph}(M_{ph}^2 - m_{ph}^2)(m_{ph}^2 + \Lambda^2)} \Big] \\
& + \frac{1}{24} \frac{g_{3ph}^2 Y_{ph}}{(4\pi)^2} \left[\frac{3\Lambda^2}{(M_{ph}^2 + \Lambda^2)^2} - \frac{1}{M_{ph}^2 + \Lambda^2} + \frac{1}{M_{ph}^2} \right]. \quad (C.6)
\end{aligned}$$

References

- [1] G. Aad, et al., Observation of a new particle in the search for the Standard Model Higgs boson with the ATLAS detector at the LHC, *Phys.Lett. B* 716 (2012) 1–29. [arXiv:1207.7214](#), [doi:10.1016/j.physletb.2012.08.020](#).
- [2] S. Chatrchyan, et al., Observation of a new boson at a mass of 125 GeV with the CMS experiment at the LHC, *Phys.Lett. B* 716 (2012) 30–61. [arXiv:1207.7235](#), [doi:10.1016/j.physletb.2012.08.021](#).
- [3] P. P. Giardino, K. Kannike, M. Raidal, A. Strumia, Reconstructing Higgs boson properties from the LHC and Tevatron data, *JHEP* 1206 (2012) 117. [arXiv:1203.4254](#), [doi:10.1007/JHEP06\(2012\)117](#).
- [4] D. Carmi, A. Falkowski, E. Kuflik, T. Volansky, J. Zupan, Higgs After the Discovery: A Status Report, *JHEP* 1210 (2012) 196. [arXiv:1207.1718](#), [doi:10.1007/JHEP10\(2012\)196](#).
- [5] T. Plehn, M. Rauch, Higgs Couplings after the Discovery, *Europhys.Lett.* 100 (2012) 11002. [arXiv:1207.6108](#), [doi:10.1209/0295-5075/100/11002](#).
- [6] L. Susskind, Dynamics of Spontaneous Symmetry Breaking in the Weinberg-Salam Theory, *Phys.Rev. D* 20 (1979) 2619–2625. [doi:10.1103/PhysRevD.20.2619](#).
- [7] G. 't Hooft, Naturalness, chiral symmetry, and spontaneous chiral symmetry breaking, *NATO Adv.Study Inst.Ser.B Phys.* 59 (1980) 135.
- [8] M. Veltman, The Infrared - Ultraviolet Connection, *Acta Phys.Polon. B* 12 (1981) 437.
- [9] H. Aoki, S. Iso, Revisiting the Naturalness Problem – Who is afraid of quadratic divergences? –, *Phys.Rev. D* 86 (2012) 013001. [arXiv:1201.0857](#), [doi:10.1103/PhysRevD.86.013001](#).
- [10] M. Farina, D. Pappadopulo, A. Strumia, A modified naturalness principle and its experimental tests, *JHEP* 1308 (2013) 022. [arXiv:1303.7244](#), [doi:10.1007/JHEP08\(2013\)022](#).
- [11] F. Jegerlehner, The Standard model as a low-energy effective theory: what is triggering the Higgs mechanism?, *Acta Phys.Polon. B* 45 (2014) 1167–1214. [arXiv:1304.7813](#), [doi:10.5506/APhysPolB.45.1167](#).
- [12] F. Jegerlehner, The hierarchy problem of the electroweak Standard Model revisited [arXiv:1305.6652](#).
- [13] L. Bian, RGE, the naturalness problem and the understanding of the Higgs mass term [arXiv:1308.2783](#).
- [14] A. de Gouvea, D. Hernandez, T. M. P. Tait, Criteria for Natural Hierarchies, *Phys.Rev. D* 89 (2014) 115005. [arXiv:1402.2658](#), [doi:10.1103/PhysRevD.89.115005](#).
- [15] S. Bar-Shalom, A. Soni, J. Wudka, EFT naturalness: an effective field theory analysis of Higgs naturalness [arXiv:1405.2924](#).

- [16] G. Passarino, M. Veltman, One Loop Corrections for $e^+ e^-$ Annihilation Into $\mu^+ \mu^-$ in the Weinberg Model, Nucl.Phys. B160 (1979) 151. doi:10.1016/0550-3213(79)90234-7.
- [17] A. Bilal, (Non) gauge invariance of Wilsonian effective actions in (supersymmetric) gauge theories: A Critical discussion, Annals Phys. 323 (2008) 2311–2348. arXiv:0705.0362, doi:10.1016/j.aop.2008.01.002.
- [18] T. Hahn, Generating Feynman diagrams and amplitudes with FeynArts 3, Comput.Phys.Comm. 140 (2001) 418–431. arXiv:hep-ph/0012260, doi:10.1016/S0010-4655(01)00290-9.
- [19] R. Mertig, M. Bohm, A. Denner, FEYN CALC: Computer algebraic calculation of Feynman amplitudes, Comput.Phys.Comm. 64 (1991) 345–359. doi:10.1016/0010-4655(91)90130-D.
- [20] A. Alloul, N. D. Christensen, C. Degrande, C. Duhr, B. Fuks, FeynRules 2.0 - A complete toolbox for tree-level phenomenology, Comput.Phys.Comm. 185 (2014) 2250–2300. arXiv:1310.1921, doi:10.1016/j.cpc.2014.04.012.
- [21] P. W. Angel, Y. Cai, N. L. Rodd, M. A. Schmidt, R. R. Volkas, Testable two-loop radiative neutrino mass model based on an $LLQd^c Qd^c$ effective operator, JHEP 1310 (2013) 118. arXiv:1308.0463, doi:10.1007/JHEP10(2013)118.
- [22] J. R. Ellis, K. Enqvist, D. V. Nanopoulos, F. Zwirner, Observables in Low-Energy Superstring Models, Mod.Phys.Lett. A1 (1986) 57. doi:10.1142/S0217732386000105.
- [23] R. Barbieri, G. Giudice, Upper Bounds on Supersymmetric Particle Masses, Nucl.Phys. B306 (1988) 63. doi:10.1016/0550-3213(88)90171-X.
- [24] D. M. Ghilencea, H. M. Lee, M. Park, Tuning supersymmetric models at the LHC: A comparative analysis at two-loop level, JHEP 1207 (2012) 046. arXiv:1203.0569, doi:10.1007/JHEP07(2012)046.
- [25] H. Gies, C. Gneiting, R. Sondenheimer, Higgs Mass Bounds from Renormalization Flow for a simple Yukawa model, Phys.Rev. D89 (2014) 045012. arXiv:1308.5075, doi:10.1103/PhysRevD.89.045012.
- [26] Z. Lalak, M. Lewicki, P. Olszewski, Higher-order scalar interactions and SM vacuum stability arXiv:1402.3826, doi:10.1007/JHEP05(2014)119.
- [27] K. Wilson, J. B. Kogut, The Renormalization group and the epsilon expansion, Phys.Rept. 12 (1974) 75–200. doi:10.1016/0370-1573(74)90023-4.
- [28] M. E. Peskin, D. V. Schroeder, An Introduction To Quantum Field Theory (Frontiers in Physics), Westview Press, 1995.
- [29] C. Wetterich, Exact evolution equation for the effective potential, Phys.Lett. B301 (1993) 90–94. doi:10.1016/0370-2693(93)90726-X.

- [30] M. Bonini, M. D’Attanasio, G. Marchesini, Perturbative renormalization and infrared finiteness in the Wilson renormalization group: The Massless scalar case, Nucl.Phys. B409 (1993) 441–464. [arXiv:hep-th/9301114](#), doi:10.1016/0550-3213(93)90588-G.
- [31] T. R. Morris, The Exact renormalization group and approximate solutions, Int.J.Mod.Phys. A9 (1994) 2411–2450. [arXiv:hep-ph/9308265](#), doi:10.1142/S0217751X94000972.
- [32] O. J. Rosten, Fundamentals of the Exact Renormalization Group, Phys.Rept. 511 (2012) 177–272. [arXiv:1003.1366](#), doi:10.1016/j.physrep.2011.12.003.
- [33] H. Gies, Introduction to the functional RG and applications to gauge theories, Lect.Notes Phys. 852 (2012) 287–348. [arXiv:hep-ph/0611146](#), doi:10.1007/978-3-642-27320-9_6.
- [34] P. Kopietz, L. Bartosch, F. Schutz, Introduction to the functional renormalization group, Lect.Notes Phys. 798 (2010) 1–380. doi:10.1007/978-3-642-05094-7.
- [35] J. Polonyi, Lectures on the functional renormalization group method, Central Eur.J.Phys. 1 (2003) 1–71. [arXiv:hep-th/0110026](#), doi:10.2478/BF02475552.
- [36] C. Bagnuls, C. Bervillier, Exact renormalization group equations. An Introductory review, Phys.Rept. 348 (2001) 91. [arXiv:hep-th/0002034](#), doi:10.1016/S0370-1573(00)00137-X.
- [37] C. Burgess, Introduction to Effective Field Theory, Ann.Rev.Nucl.Part.Sci. 57 (2007) 329–362. [arXiv:hep-th/0701053](#), doi:10.1146/annurev.nucl.56.080805.140508.
- [38] H. Sonoda, Wilson’s renormalization group and its applications in perturbation theory [arXiv:hep-th/0603151](#).
- [39] M. Bonini, M. D’Attanasio, Spontaneous symmetry breaking with Wilson renormalization group, Nucl.Phys. B466 (1996) 315–334. [arXiv:hep-th/9507098](#), doi:10.1016/0550-3213(96)00073-9.
- [40] U. Ellwanger, The Running gauge coupling in the exact renormalization group approach, Z.Phys. C76 (1997) 721–727. [arXiv:hep-ph/9702309](#), doi:10.1007/s002880050593.
- [41] A. Strumia, Naturalness of supersymmetric models [arXiv:hep-ph/9904247](#).
- [42] G. W. Anderson, D. J. Castano, Measures of fine tuning, Phys.Lett. B347 (1995) 300–308. [arXiv:hep-ph/9409419](#), doi:10.1016/0370-2693(95)00051-L.
- [43] J. Polchinski, Renormalization and Effective Lagrangians, Nucl.Phys. B231 (1984) 269–295. doi:10.1016/0550-3213(84)90287-6.
- [44] K. Nishijima, M. Okawa, Renormalization in a symmetry broken theory, Prog.Theor.Phys. 61 (1979) 1822. doi:10.1143/PTP.61.1822.
- [45] H. Arason, D. Castano, B. Keszthelyi, S. Mikaelian, E. Piard, et al., Renormalization group study of the standard model and its extensions. 1. The Standard model, Phys.Rev. D46 (1992) 3945–3965. doi:10.1103/PhysRevD.46.3945.

- [46] C. Ford, D. Jones, P. Stephenson, M. Einhorn, The Effective potential and the renormalization group, Nucl.Phys. B395 (1993) 17–34. [arXiv:hep-lat/9210033](#), [doi:10.1016/0550-3213\(93\)90206-5](#).
- [47] H. Gies, R. Sondenheimer, Higgs Mass Bounds from Renormalization Flow for a Higgs-top-bottom model [arXiv:1407.8124](#).